ORIGINAL ARTICLE

Potential inhibitors of methionine aminopeptidase type II identified via structure-based pharmacophore modeling
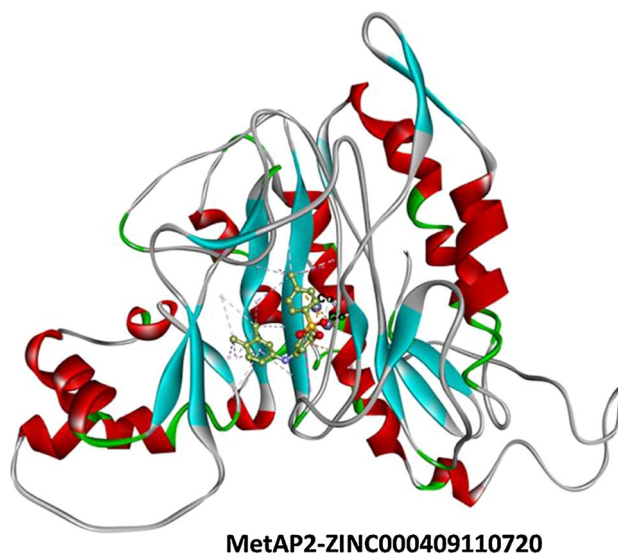
Safana Albayati[1] · Abdullahi Ibrahim Uba[1,2] · Kemal Yelekçi[1]

Abstract

Methionine aminopeptidase (MetAP2) is a metal-containing enzyme that removes initiator methionine from the N-terminus of a newly synthesized protein. Inhibition of the enzyme is crucial in diminishing cancer growth and metastasis. Fumagillin—a natural irreversible inhibitor of MetAP2—and its derivatives are used as potent MetAP2 inhibitors. However, because of their adverse effects, none of them has progressed to clinical studies. In search for potential reversible inhibitors, we built structure-based pharmacophore models using the crystal structure of MetAP2 complexed with fumagillin (PDB ID: 1BOA). The pharmacophore models were validated using Gunner–Henry scoring method. The best pharmacophore consisting of 1 H-bond donor, 1 H-bond acceptor, and 3 hydrophobic features was used to conduct pharmacophore-based virtual screening of ZINC15 database against MetAP2. The top 10 compounds with pharmacophore fit values > 3.00 were selected for further analysis. These compounds were subjected to absorption, distribution, metabolism, elimination, and toxicity (ADMET) prediction and found to have druglike properties. Furthermore, molecular docking calculations was performed on these hits using AutoDock4 to predict their binding mode and binding energy. Three diverse compounds: ZINC000014903160, ZINC000040174591, and ZINC000409110720 with respective binding energy/docking scores of − 9.22, − 9.21, and −817 kcal/mol, were submitted to 100 ns (MD) simulations using Nanoscale MD (NAMD) software. The compounds showed stable binding mode over time. Therefore, they may serve as a scaffold for further computational and experimental optimization toward the design of more potent and safer MetAP2 inhibitors.

Graphic abstract

MetAP2-ZINC000409110720

Safana Albayati and AbdullahiIbrahim Uba have contributed equally.

Extended author information available on the last page of the article

🖄 Springer

Introduction

Methionine aminopeptidase (MetAPs) is a metal-containing enzyme that cleaves the N-terminal initiator methionine from a number of newly synthesized protein—this step is required for a correct protein folding and function [1]. There are three known mammalian MetAPs: MetAP1, MetAP2, and MetAP3 (MAP1D). MetAP1 and MetAP2 are found in eukaryotes, while MetAP1 is expressed in procaryotes. MetAP2 plays a critical role in the growth of new blood vessels (angiogenesis) in cancers [2], and regulation of adipose tissue in obesity through vasculature [3]. Fumagillin and its derivative TNP-470 are potent and selective natural inhibitors of MetAP2. Fumagillin and TNP470, potent and selective natural inhibitors of MetAP2, covalently bind to MetAP2 and block neovascularization via endothelial cell cycle arrest in the late G1 phase [1, 2, 4]. However, the U.S. Food and Drug Administration (FDA) found the biomolecule inadmissible in clinical trials due to its toxicity. To date, no drugs have been approved targeting MetAP2, hence active search for MetAP2 inhibitors is needed.

Studies have shown that rational drug design approach could be successfully applied to specifically target the enzyme for the treatment of cancers [5, 6], obesity [7–9], and other diseases. Toward this goal, combinations of computational and experimental methods have proven to be fast and effective [10, 11]. To treat obesity condition, Cheruvallath and coworkers employed a combination of fragment-based and structure-based drug discovery methods to design potent (< 10 nM) indazoles that showed reversible MetAP2 inhibition at nanomolar concentration [12]. In continuation with their studies, the group derived more potent, selective, and orally available MetAP2 inhibitors from pyrazolo[4,3-b]indole core using SAR and accelerated knowledge-based fragment growth; and treatment with these inhibitors led to robust and sustainable body weight loss in DIO mice [13]. A potent and reversible MetAP-2 inhibitor, M8891, discovered via structure-based hit optimization, impeded the growth of primary endothelial cells and showed antitumoral activity in mouse models [14]. Recently, using a combined computational molecular design approach, our group identified potential MetAP2 inhibitors [15]. Therefore, these studies and more [16] show that computational methods are powerful tools that aid in the search for potent, selective, and reversible MetAP2 inhibitors; and their potential use to treat a variety of cancers, and obesity condition.

Here, in search for reversible inhibitors of MetAP2, structure-based pharmacophore models were built from the crystal structure of MetAP2 complexed with fumagillin (PDB ID: 1BOA)[17], and validated using Güner–Henry scoring method [18]. The best model (hypothesis 1) was used to conduct pharmacophore-based virtual screening of ZINC15 druglike database. Top hits with pharmacophore fit values > 3.00 were studied using molecular docking. To examine the stability of ligand binding mode, MetAP2 complexes with fumagillin and diverse compound (ZINC000014903160, ZINC000040174591, and ZINC000409110720) from the top 10 hits were submitted to molecular dynamic simulation. These compounds were found to be stable in the active site of MetAP2, with similar orientation to that of the cocrystal ligand fumagillin. Therefore, we suggest these compounds to be potential MetAP2 inhibitors, subject to further computational and experimental optimization.

Methods

Structure-based pharmacophore generation

Crystal structures of MetAP2 complexed with angiogenesis inhibitor fumagillin (PDB ID: 1BOA; Resolution: 1.80 Å [17] was retrieved from the protein data bank (PDB) [19]. The complex was prepared using the "Protein preparation toolkit" available in Biovia Discovery Studio 4.5. Subsequently, 10 structure-based pharmacophore models (hypotheses) were built using "Receptor-based pharmacophore" generation toolkit of Biovia Discovery Studio 4.5. The pharmacophore models were subjected to evaluation as described in the following section.

Pharmacophore model validation

A total of 39 known MetAP2 inhibitors, whose experimental activity values and sources are shown in Table S1, were retrieved [20–32]. A total of 1842 inactive (decoys) compounds were generated using the Directory of Useful Decoys-Enhanced (http://dude.docking.org/) [33]. Hence, a database containing 39 active and 1842 inactive molecules was built and used to evaluate the discriminative ability of the pharmacophore model in distinguishing active compounds from the inactive compounds. The database screening was performed using the pharmacophore database search available in Biovia Discovery Studio 4.5. The Güner–Henry scoring method was used to evaluate the ability of the generated models to selectively retrieve active molecules from a dataset containing known active and inactive molecules.

The following equation was used to compute the goodness-of-hit score:

$$\%A = \frac{Ha}{A}$$

$$\%Y = \frac{Ha}{Ht} * 100$$

$$E = \frac{Ha/Ht}{A/D}$$

$$GH = \left(\frac{Ha(2A + Ht)}{4HtA}\right)\left(1 - \frac{Ht - Ha}{D - A}\right).$$

The total hits is (Ht), number of active molecules (A), number of active hit (Ha), % active of actives (%A), yield of actives (%Y), enrichment factor (E), and goodness-of-hit score (GH). The GH score ranges from 0 to 1, which indicates a null model and an ideal model, respectively [18, 34].

Pharmacophore-based virtual screening

Hypo1 consisting of 1 H-bond donors, 1 H-bond acceptors, and 3 hydrophobic features (ADHHH) and Hypo2 consisting of 2 H-bond acceptors and 3 hydrophobic features (AAHHH), both from 1BOA complex, were found to have the highest GH score (0.92). A GH score between 0.6 and 1.00 suggests robustness of a pharmacophore hypothesis [18]. Hypo1 was selected based on feature diversity and used to conduct pharmacophore-based virtual screening of ZINC15 database containing over two hundred and 230,000,000 commercially available compounds, freely accessible for download [35]. To reduce this huge database to a manageable number, filtration was done based on "Lipinski's rule of 5": logP ≤ 5, molecular weight: 250 to 500 Da, number of H-bond donors ≤ 5; number of H-bond acceptors ≤ 10; [36], and number of rotatable bonds ≤ 4 [37]. A reduced database containing 6,000,000 compounds was built in Biovia DS 4.5, and Hypo1 was run against it. The top 10 compounds—all with pharmacophore fit value of > 3.00—were saved for further analysis.

Molecular docking

AutoDockTools [38] was used to assign partial charges to each atom to generate "protein.pdbqt". The Zinc charge in this file was manually modified to + 2. Energy grid boxes of dimensions 70, 70, and 70 Å were used to cover the entire binding site of MetAP2 and its neighboring residues. The grid dimension was adopted from our previous study on computational identification of MetAP2 inhibitor [15].

AutoDock 4.2′s Lamarckian genetic algorithm in AutoDock4 [38] was used for ligand conformational search, with 20 independent runs and 20,000,000 energy evaluations for each ligand.

Druglike and ADMET prediction

Even though the database was initially developed based on Druglikeness, further prediction based on Lipinski's "Rule of 5" [36, 37], AdmetSAR server was used again to evaluate the top 10 hit compounds. This server calculates ADMET properties based on substructure pattern recognition using support vector machine algorithm [39].

Molecular dynamics simulation

The MetAP2 docking complexes with the pharmacophore best-fitting compounds (ZINC000014903160, ZINC000040174591, and ZINC000409110720) were prepared for MD simulation. As a control, the crystal structure of MetAP2 complexed with fumagillin (1BOA) was also prepared for MD simulation. Input files were generated using CHARMM-GUI server (http://www.charmm.org)[40], via which the ligands were parameterized using CHARMM General Force Field (CGenFF) server (https://cgenff.param chem.org/) [41]. MD simulation was performed using Nanoscale MD (NAMD) software [42]. For each system, the following simulation protocols were applied: 1000 steps of minimization by steepest descent method; 5 ns equilibration in standard number of particles, volume, and temperature (NVT) ensemble; and unrestrained 200 ns-production MD simulations in standard number of particles, pressure, and temperature (NPT) ensemble. The simulation was carried out at 2 fs time scale, and the trajectory frame was collected every 20 ps. To identify the most populated structure representing each system, the trajectories were clustered using RMSD cutoff of 2.5 Å in Chimera [43]. The stability of each system was assessed by computing the root mean-square deviation (RMSD) and root mean-square fluctuation (RMSF) over the entire simulation period.

Results and discussion

Redocking of the cocrystal ligand

To validate the docking algorithm employed, the cocrystal ligand fumagillin was redocked into the active site of MetAP2 using docking procedure described in molecular docking subsection above. The docked and crystal poses of fumagillin overlaid in the active site of MetAP2, aligned well with each other with RMSD value of 0.92 Å (Fig. 1).

Fig. 1 Molecular overlay of the cocrystal ligand (Fumagillin) (Pink) with its docked pose (Green) in the active site of MetAP2. The RMSD between the crystal and docked poses is found to be 0.92 Å
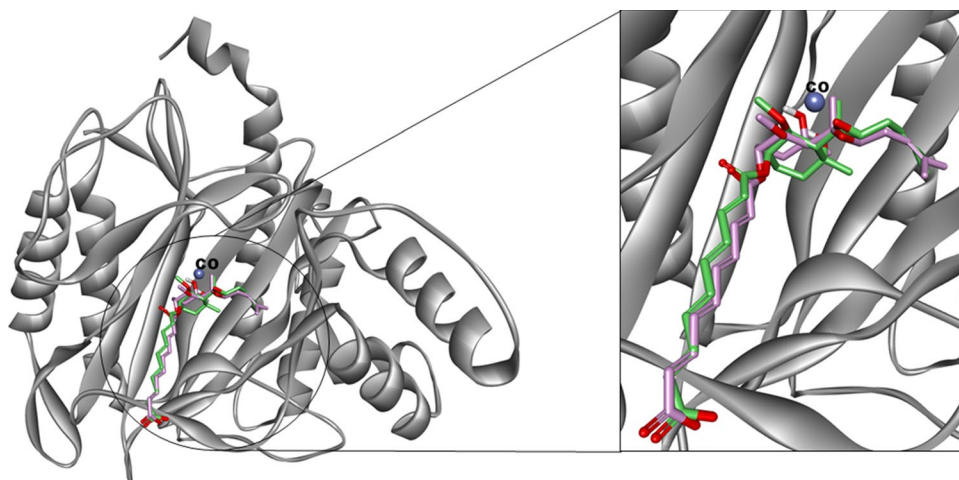
Pharmacophore models generated

The 10 pharmacophores hypotheses generated, their features, selectivity, and GH scores are given in Table 1. Hypothesis 1 (Hypo1) and hypothesis 2 (Hypo2) were found to have same GH score, despite consisting of different set of features. Hyop1 consists of 1 H-bond donors, 1 H-bond acceptors, and 3 hydrophobic features (ADHHH) and displayed the highest selectivity (Fig. 2). A pharmacophore model with high selectivity tends to retrieve compounds that fit well protein binding pocket [44, 45].

Predicted binding affinity of best-fitting compounds

The top 10 compounds were found to have pharmacophore fit values > 3.00. Compounds with pharmacophore fit values > 3.00 have been shown by our previous data [45] and those of others [46] to have good inhibition potential against respective targets. The predicted binding affinities of the top 10 hit compounds are ranked from highest to lowest—in

comparison with that of the cocrystal ligand, fumagillin. The chemical structures of the diverse compounds are available in the supplementary materials (Table S1). The binding affinity of the best pose out of 20 generated docking poses for each compound is presented in Table 2. Compounds submitted to MD simulations were selected based on binding affinity and scaffold diversity.

Protein–Ligand interaction

Figure 2 shows the detailed interactions between MetAP2 and ZINC000014903160 (Fig. 3a), ZINC000040174591 (Fig. 3b), and ZINC000409110720 (Fig. 3c). The 3D and 2D representations are provided in the left and right panels, respectively. ZINC000014903160 spanned the active site of MetAP2 by forming strong metallic interaction with Co^{2+} ion via thiophene group; phi–cation interactions with His231 and His331; H-bond with Glu364, several hydrophobic interactions, and a couple of other interactions. The binding orientation of ZINC000014903160 and its

Table 1 Pharmacophore models and validation

Hypothesis	Features	Selectivity	D	A	Ht	Ha	%A	%Y	E	GH
1	ADHHH	8.9325	1881	39	31	30	76.92	96.77	46.674	0.917615711
2	AAHHH	8.0189	1881	39	31	30	76.92	96.77	46.674	0.917615711
3	ADHH	7.4177	1881	39	31	29	74.36	93.54	45.119	0.886546701
4	ADHH	7.4177	1881	39	38	31	79.49	81.57	39.346	0.80747975
5	ADHH	7.4177	1881	39	39	31	79.49	79.48	38.337	0.791419583
6	DHHH	7.4177	1881	39	39	30	76.92	76.92	37.101	0.765472313
7	AAHH	6.5041	1881	39	38	31	79.49	81.57	39.346	0.80747975
8	AAHH	6.5041	1881	39	34	28	71.79	82.35	39.719	0.79453771
9	AAHH	6.5041	1881	39	38	31	79.49	81.57	39.346	0.80747975
10	AHHH	6.5041	1881	39	34	30	76.923	88.23	42.557	0.852217735

H-bond donor (D); H-bond acceptor (A), Hydrophobic feature (H), total hits (Ht), number of active molecules (A), number of active hit (Ha), % active of actives (%A), yield of actives (%Y), enrichment factor (E), and goodness-of-hit score (GH). The GH score ranges from 0 to 1, which indicates a null model and an ideal model, respectively
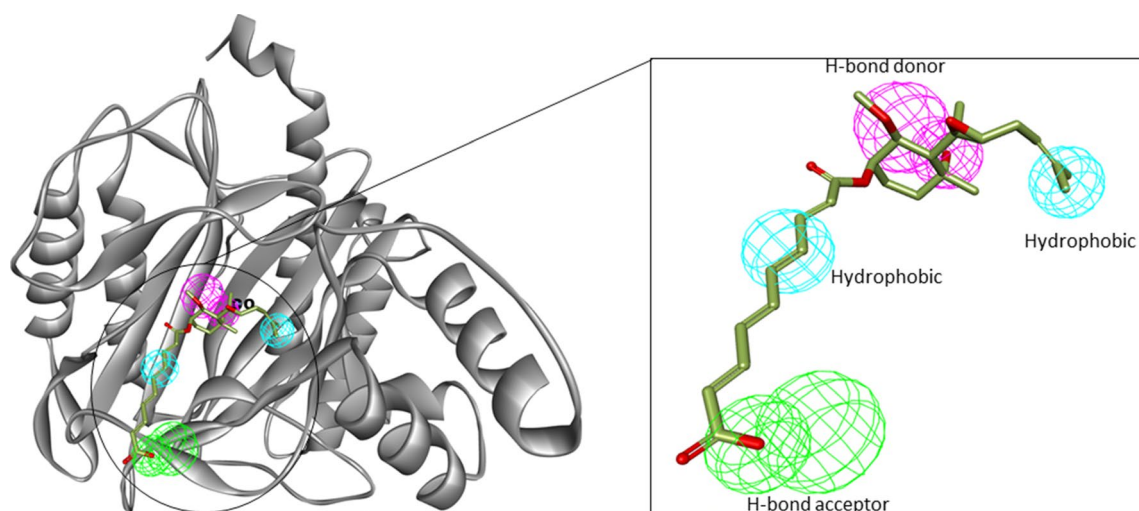
Fig. 2 The best pharmacophore hypotheses generated using 1BOA complex: H-bond donor (Purple); H-bond acceptor (Green); Hydrophobic feature (Cyan). Hyop1 consists of 1 H-bond donors, 1 H-bond acceptors, and 3 hydrophobic features (ADHHH)

interactions may be correct enough to stabilize the complex. In case of ZINC000409110720, the Co^{2+} ion was engaged with imidazole group via metal–acceptor interaction. Other types of interaction include a H-bond with His331, a couple of hydrophobic and van der Waal's interactions, phi–phi T-shaped and phi–sigma interactions. Fore MetAP2- ZINC000409110720 complex, Co^{2+} ion was not involved interactions—rather a strong H-bond was formed between the sulfonyl group and Asn329, and a phi–cation interaction between the central aromatic linker and His331. Other interactions include several hydrophobic interactions, a phi–phi T-shaped and a phi–sigma interaction. These interactions added up to give the overall strong binding affinity observed in these ligands.

Predicted ADMET and druglike properties

The top 10 hit compounds showed potentialities to be druglike having obeyed Lipinski's "Rule of 5" [36] and other physicochemical properties. All the physicochemical parameters were found to be within the range of orally available drug molecules (Table 3). Caco-2 cells permeability is a model of human intestinal absorption of drugs and other compounds [47]. Aqueous solubility is an important physicochemical property that determines the uptake, and the distribution, metabolism, and elimination (ADME) characteristics of a molecule [48].

Figure 4 shows ADMET plot of PSA (polar surface area) versus AlogP98 (n-octanol–water the logarithm of the partition coefficient). The ellipses enclose regions where well-absorbed compounds are expected to be found. About 95 and 99% of well-absorbed compound are expected to be within the ellipses colored in red and

green, respectively, for intestinal absorption. Similarly, for the blood–brain barrier penetration, 95 and 99% of well-absorbed inhibitors are expected to fall within the ellipses colored with magenta and aqua, respectively. Here, all the 10 hits are enclosed inside all four ellipses, satisfying the conditions for absorption by the intestines and the brain.

Predicting and assessing the bioactivity of the 10 compounds

Bioactivity of a compound is essential for assessing lead-likeness of a compound. Bioactivity prediction was recently applied to study potential inhibitors of MetAP2 [15]. In this study, the following parameters were calculated: ligand efficiency (LEF), LEF scale, fit quality (FQ), and LEF-dependent lipophilicity (LEFDL) (Table 4) [49].

$$LEF = \frac{-BF}{NHA}.$$

NHA is the number of heavy atoms in a molecule. BF is the ratio of the binding affinity.

Scaling function (LEF scale) is derived by fitting an exponent function for maximizing LEF values observed for a given NHA count:

$$LEF_{Scale} = 0.873 \times e^{-0.026 \times NHA} - 0.064.$$

FQ is the quotient of the observed LEF and the LEF scale and is given by:

$$FQ = \frac{LEF}{LEF \, scale}.$$

LEFDL is the ratio of the log p to the LEF computed as:

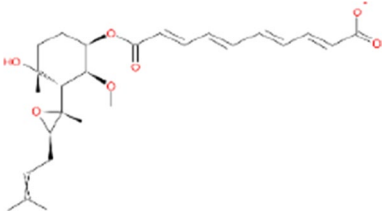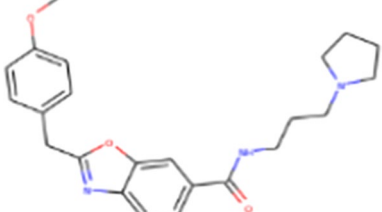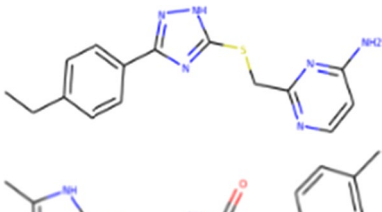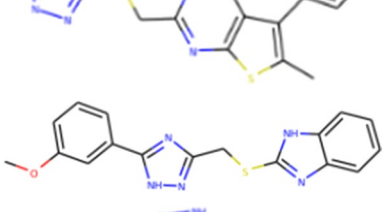**Table 2** Calculated binding affinity of the best 10 compounds
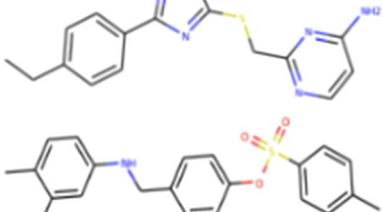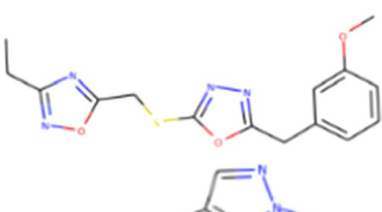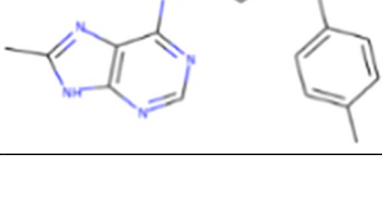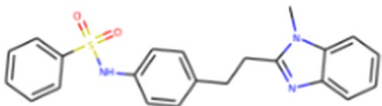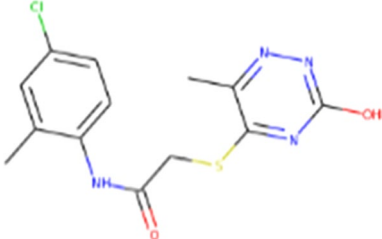
Compound	Structure	Pharmacophore fit value	ΔG (Kcal/mol)
Fumagillin		4.21	− 9.20
ZINC000048988425		3.98	− 10.01
ZINC000064968449		3.95	− 9.24
ZINC000014903160		3.92	− 9.22
ZINC000040174591		3.86	− 9.21
ZINC000095431249		3.84	− 8.49
ZINC000409110720		3.65	− 8.37
ZINC000066256921		3.33	− 8.19
ZINC000046087785		3.30	− 8.13

Table 2 (continued)

Compound	Structure	Pharmacophore fit value	ΔG (Kcal/mol)
ZINC000015870630		3.21	− 8.11
ZINC000015831093		3.01	− 8.10

$$LEFDL = \frac{\log p}{LEF}.$$

When LEF > 0.3, FQ score increases and the affinity of the final compound approaches near optimal state. An LEFDL value > 3 suggests optimal compound [49].

Molecular dynamics simulation

A total of 4 systems (MetAP2 complexes with fumagillin, and with 3 compounds: ZINC000014903160, ZINC000040174591, and ZINC000409110720) were submitted to unrestrained 200 MD simulation. These 3 hit compounds were selected from the top 10 best-fitting compounds based on structural diversity.

RMSD is a commonly used measure of similarity between two protein structures, which in turn suggests structural stability [50]. Here, all frames were aligned with the initial structure and the resulting RMSD was computed. The RMSD of the 4 systems varied between 0 and 4.2 Å until around 100 ns, and then converged to about 2.8 to 3.4 Å for the MetAP2 complexes with the 3 hit compounds until the end of the simulation. On the other hand, the MetAP2-fumagillin complex reached RMSD convergence (between 3.2 and 4.0 Å) beyond 130 ns (Fig. 5a). The backbone root mean-square fluctuation (RMSF) is a measure of the displacement of a particular atom, or group of atoms (residue), relative to the reference structure, averaged over the number of atoms [51]. The RMSF is another parameter used to assess protein structural stability. The RMSF profiles of all the systems showed similar trends with the RMSD variations, although few residues away from the active site showed increased fluctuation (Fig. 5b). Therefore, these results suggest potentialities of the proposed compounds to form stable complexes with MetAP2.

Conclusion

Inhibition of MetAP2 has been shown to be promising for the treatment of cancers and obesity condition. In search for reversible MetAP2 inhibitors, structure-based pharmacophore models were developed and used to screen a ZINC15 database. The top hit compounds were filtered based on pharmacophore fit criteria (Fit value > 3.00). The 10 best-fitting compounds subjected to ADMET and bioactivity predictions were found to be druglike and efficient. Henceforth, 3 compounds (ZINC000014903160, ZINC000040174591, and ZINC000409110720) selected from the best-fitting compounds based on diversity were docked to the active site of MetAP2 and then subjected to all-atom MD simulation, with the crystal structure of MetAP2-fumagillin complex (1BOA) as positive control. These compounds demonstrate potential stability in the active site of MetAP2 over time. They may therefore serve as additional scaffolds for further optimization toward the design of more potent and safer MetAP2 inhibitors.
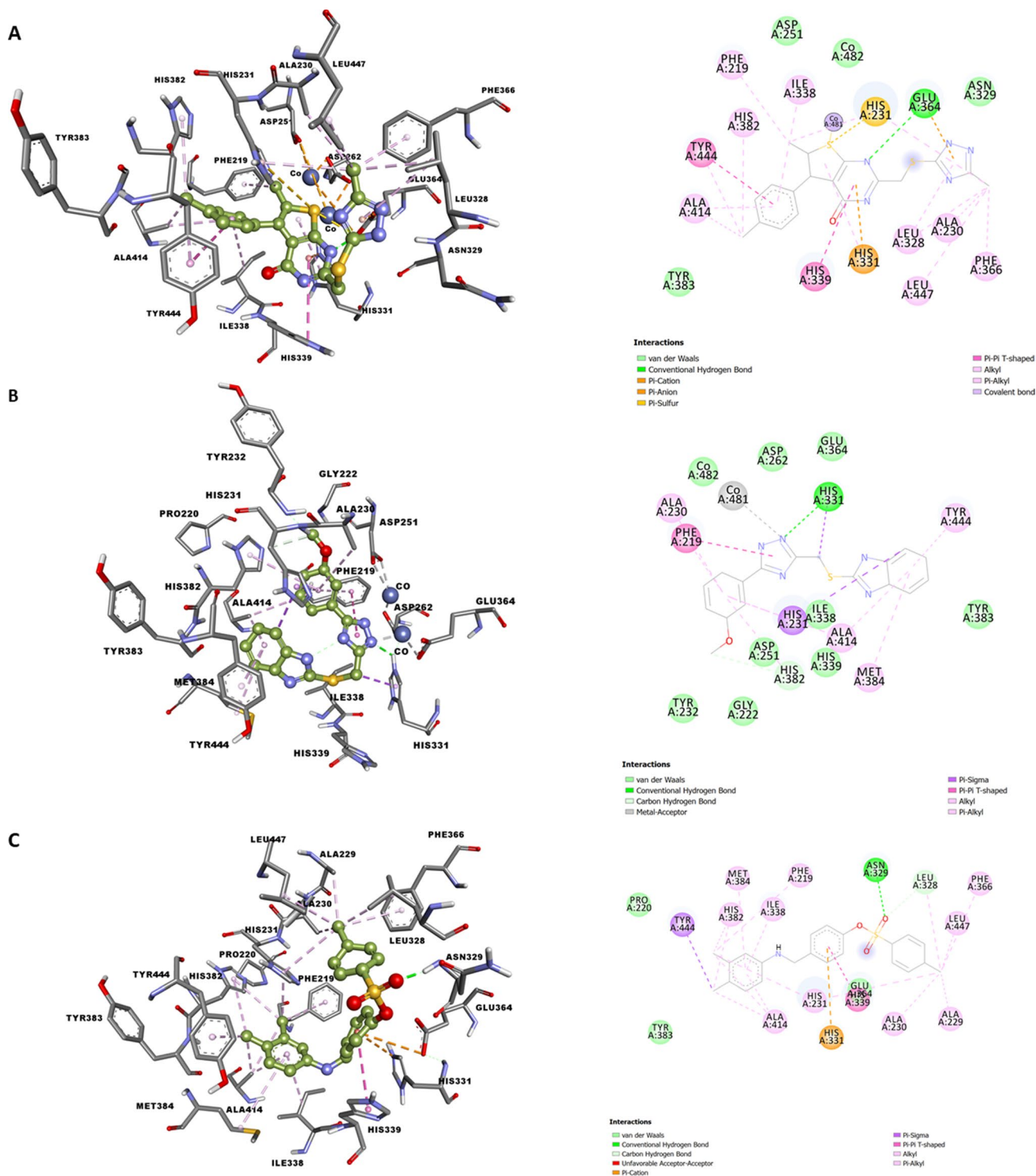
Fig. 3 Interaction between MetAP2 and ligands. **a** ZINC000014903160. **b** ZINC000040174591. **c** ZINC000409110720. 3D and 2D interaction representations are shown in the left and right panels, respectively

Table 3 Predicted ADMET and druglike properties of the top 10 hit compounds

Compound	Mol. Weight (Da)	LogP	TPSA (Å²)	Rotatable Bonds	H-Bond Donor	H-Bond Acceptor	Aqueous solubility (LogS)	Caco-2 permeability (LogPapp, cm/s)
ZINC000048988425	425.9	2.965	91	4	2	5	−4.057	0.7462
ZINC000064968449	393.5	3.643	68	8	2	4	−2.84	0.6965
ZINC000014903160	383.5	3.987	87	4	2	6	−3.48	0.5895
ZINC000040174591	337.5	3.649	79	5	2	5	−3.317	0.6380
ZINC000095431249	312.4	2.699	93	5	2	6	−2.461	0.5625
ZINC000409110720	381.5	4.992	55	6	1	4	−4.012	0.5648
ZINC000066256921	332.4	2.907	87	7	0	8	−2.899	0.6259
ZINC000046087785	319.37	2.958	84	4	2	6	−3.13	0.5784
ZINC000015870630	391.5	4.159	63	6	1	4	−3.662	0.6356
ZINC000015831093	324.8	2.578	87	4	2	5	−3.681	0.5174

LogP (Octanol–water partition coefficient) ≤ 5; Molecular weight ≤ 500 Da; H-Bond Donor ≤ 5. H-Bond Acceptor ≤ 5. T_PSA (Topological polar surface area) ≤ 140 Å². P(BBB +) (Probability for blood–brain barrier penetration). Aqueous solubility (LogS ≥ −5.7). Caco-2 permeability > 22 nm/s

Fig. 4 Predicted ADMET and druglike properties of the top 10 hit compounds. All the 10 hits are enclosed inside all four ellipses, satisfying the conditions for absorption by the intestines and the brain
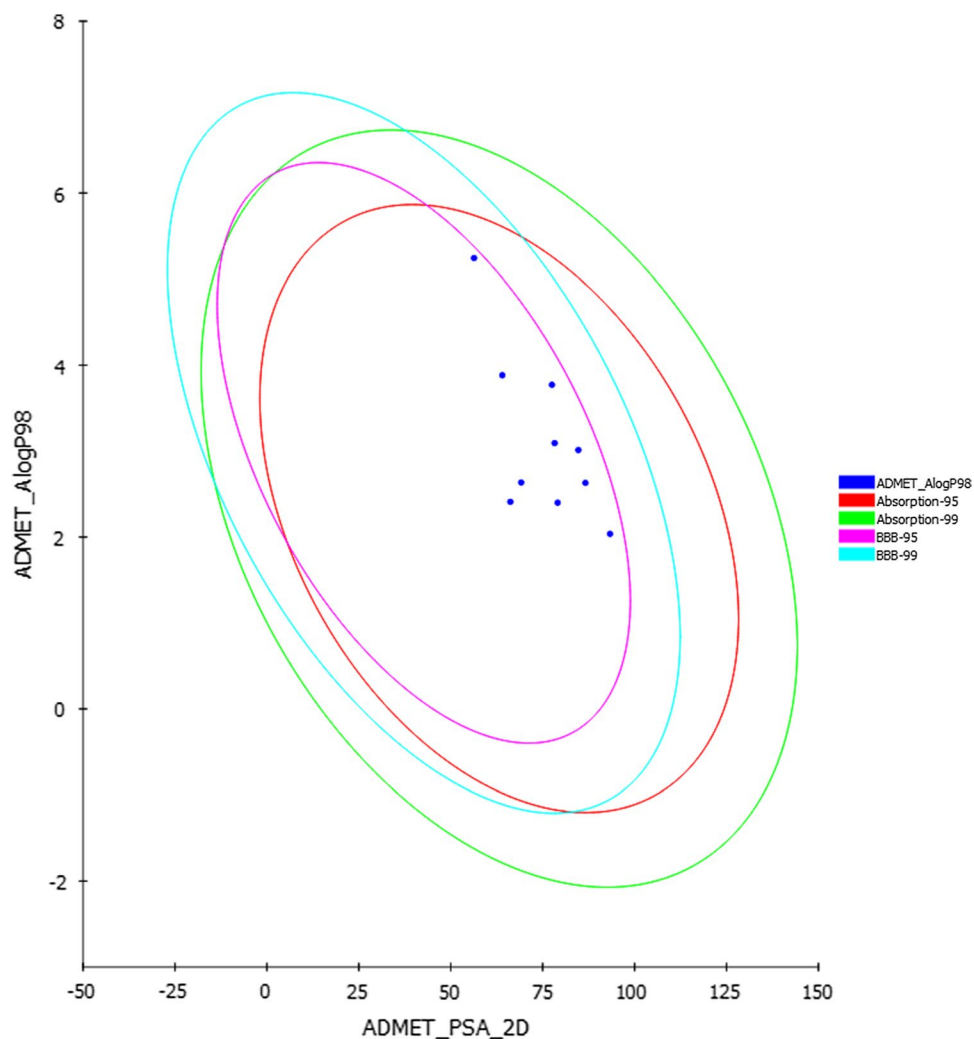
Table 4 Bioactivity and efficiency parameters of the top 10 hit compounds

Compound	BF	NHA	LEF	LEF Scale	FQ	LEFDL
ZINC000048988425	10.88	30	0.362667	0.336188448	1.078761	8.161757
ZINC000064968449	9.96	29	0.343448	0.346729791	0.990535	10.5984
ZINC000014903160	9.31	26	0.358077	0.380049284	0.942186	11.13448
ZINC000040174591	9.75	24	0.40625	0.403750744	1.00619	8.982154
ZINC000095431249	9.02	22	0.41	0.428717287	0.956341	6.582927
ZINC000409110720	9.77	27	0.361852	0.368652799	0.981552	13.7957
ZINC000066256921	9.91	23	0.43087	0.416071742	1.035567	6.746815
ZINC000046087785	9.03	24	0.37625	0.403750744	0.931887	7.861794
ZINC000015870630	10.65	28	0.380357	0.357548803	1.06379	10.93446
ZINC000015831093	9.02	21	0.429524	0.441695928	0.972443	6.001993

When LEF > 0.3, FQ score increases; the affinity of the final compound approaches near optimal affinity. An LEFDL value > 3 suggests optimal compound
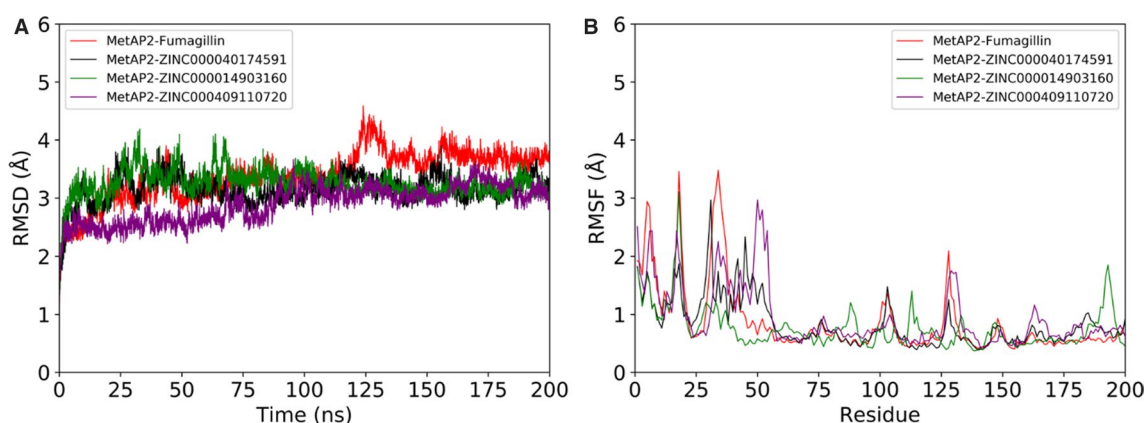

Fig. 5 Molecular dynamics simulation of MetAP2 in complex with fumagillin, ZINC000014903160, ZINC000040174591, and ZINC000409110720: (A) Root mean-square deviation (RMSD) (B) Root mean-square fluctuation (RMSF)

Declarations

Conflict of interest The authors indicate no potential conflicts of interest.

References

1. Griffith EC et al (1998) Molecular recognition of angiogenesis inhibitors fumagillin and ovalicin by methionine aminopeptidase 2. Proc Natl Acad Sci 95(26):15183–15188. https://doi.org/10.1073/pnas.95.26.15183
2. O'Reilly MS, Brem H, Folkman J (1995) Treatment of murine hemangioendotheliomas with the angiogenesis inhibitor AGM-1470. J Pediatr Surg 30(2):325–330. https://doi.org/10.1016/0022-3468(95)90583-9
3. Rupnick MA et al (2002) Adipose tissue mass can be regulated through the vasculature. Proc Natl Acad Sci U S A 99(16):10730–10735. https://doi.org/10.1073/pnas.162349799
4. Takamiya Y et al (1994) AGM-1470 inhibits the growth of human glioblastoma cells in vitro and in vivo. Neurosurgery 34(5):869–875. https://doi.org/10.1227/00006123-199405000-00013
5. Yin SQ et al (2012) The development of MetAP-2 inhibitors in cancer treatment. Curr Med Chem 19(7):1021–1035. https://doi.org/10.2174/092986712799320709
6. Esa R et al (2020) The role of methionine Aminopeptidase 2 in Lymphangiogenesis. Int J Mol Sci. https://doi.org/10.3390/ijms21145148
7. McCandless SE et al (2017) Effects of MetAP2 inhibition on hyperphagia and body weight in Prader-Willi syndrome: a randomized, double-blind, placebo-controlled trial. Diabetes Obes Metab 19(12):1751–1761. https://doi.org/10.1111/dom.13021
8. Siddik MAB et al (2019) A MetAP2 inhibitor blocks adipogenesis, yet improves glucose uptake in cells. Adipocyte 8(1):240–253. https://doi.org/10.1080/21623945.2019.1636627
9. Proietto J et al (2018) Efficacy and safety of methionine aminopeptidase 2 inhibition in type 2 diabetes: a randomised,

placebo-controlled clinical trial. Diabetologia 61(9):1918–1922. https://doi.org/10.1007/s00125-018-4677-0

10. Han Mİ et al (2019) Synthesis, molecular modeling, in vivo study, and anticancer activity of 1,2,4-triazole containing hydrazide–hydrazones derived from (S)-naproxen. Archiv der Pharmazie. https://doi.org/10.1002/ardp.201800365

11. Yılmaz Ö et al (2020) Synthesis, anticancer activity on prostate cancer cell lines and molecular modeling studies of flurbiprofen-thioether derivatives as potential target of metap (type II). Med Chem 16(6):735–749. https://doi.org/10.2174/15734064156661 90613162322

12. Cheruvallath Z et al (2016) Discovery of potent, reversible MetAP2 inhibitors via fragment based drug discovery and structure based drug design—part 1. Bioorg Med Chem Lett 26(12):2774–2778. https://doi.org/10.1016/j.bmcl.2016.04.073

13. McBride C et al (2016) Discovery of potent, reversible MetAP2 inhibitors via fragment based drug discovery and structure based drug design-Part 2. Bioorg Med Chem Lett 26(12):2779–2783. https://doi.org/10.1016/j.bmcl.2016.04.072

14. Heinrich T et al (2019) Identification of Methionine Aminopeptidase-2 (MetAP-2) Inhibitor M8891: a clinical compound for the treatment of cancer. J Med Chem 62(24):11119–11134. https://doi.org/10.1021/acs.jmedchem.9b01070

15. Weako J et al (2020) Identification of potential inhibitors of human methionine aminopeptidase (type II) for cancer therapy: structure-based virtual screening, ADMET prediction and molecular dynamics studies. Comput Biol Chem. https://doi.org/10.1016/j.compbiolchem.2020.107244

16. Heinrich T et al (2017) Novel reversible methionine aminopeptidase-2 (MetAP-2) inhibitors based on purine and related bicyclic templates. Bioorg Med Chem Lett 27(3):551–556

17. Liu S et al (1998) Structure of human methionine aminopeptidase-2 complexed with fumagillin. Science 282(5392):1324–1327. https://doi.org/10.1016/j.bmcl.2016.12.019

18. Guner O, Clement O, Kurogi Y (2004) Pharmacophore modeling and three dimensional database searching for drug design using catalyst: recent advances. Curr Med Chem 11(22):2991–3005. https://doi.org/10.2174/0929867043364036

19. Berman HM et al (2000) The protein data bank. Nucleic Acids Res 28(1):235–242

20. Çoruh I et al (2018) Synthesis, anticancer activity, and molecular modeling of etodolac-thioether derivatives as potent methionine aminopeptidase (type II) inhibitors. Archiv der Pharmazie. https://doi.org/10.1093/nar/28.1.235

21. Liu T et al (2010) Differential expression profiles of alternaria alternate genes in response to carbonyl sulfide fumigation. J Microbiol 48(4):480–485. https://doi.org/10.1007/s12275-010-9301-z

22. Kusaka M et al (1991) Potent anti-angiogenic action of AGM-1470: comparison to the fumagillin parent. Biochem Biophys Res Commun 174(3):1070–1076. https://doi.org/10.1016/0006-291x(91)91529-l

23. Arico-Muendel CC et al (2009) Carbamate analogues of fumagillin as potent, targeted inhibitors of methionine aminopeptidase-2. J Med Chem 52(24):8047–8056. https://doi.org/10.1021/jm901260k

24. Kass DJ et al (2012) Early treatment with fumagillin, an inhibitor of methionine aminopeptidase-2, prevents pulmonary hypertension in monocrotaline-injured rats. PLoS ONE 7(4):e35388. https://doi.org/10.1371/journal.pone.0035388

25. Ehlers T et al (2016) Methionine aminopeptidase type-2 inhibitors targeting angiogenesis. Curr Top Med Chem 16(13):1478–1488. https://doi.org/10.2174/1568026615666150915121204

26. Bernier SG et al (2004) A methionine aminopeptidase-2 inhibitor, PPI-2458, for the treatment of rheumatoid arthritis. Proc Natl Acad Sci U S A 101(29):10768–10773. https://doi.org/10.1073/pnas.0404105101

27. Sheppard GS et al (2004) 3-Amino-2-hydroxyamides and related compounds as inhibitors of methionine aminopeptidase-2. Bioorg Med Chem Lett 14(4):865–868

28. Kallander LS et al (2005) 4-Aryl-1,2,3-triazole: a novel template for a reversible methionine aminopeptidase 2 inhibitor, optimized to inhibit angiogenesis in vivo. J Med Chem 48(18):5644–5647. https://doi.org/10.1016/j.bmcl.2003.12.031

29. Wang GT et al (2007) Lead optimization of methionine aminopeptidase-2 (MetAP2) inhibitors containing sulfonamides of 5,6-disubstituted anthranilic acids. Bioorg Med Chem Lett 17(10):2817–2822. https://doi.org/10.1016/j.bmcl.2007.02.062

30. Kawai M (2006) Development of sulfonamide compounds as potent methionine aminopeptidase type II inhibitors with antiproliferative properties. Bioorg Med Chem Lett 16(13):3574–3577. https://doi.org/10.1016/j.bmcl.2006.03.085

31. Marino JP Jr et al (2007) Highly potent inhibitors of methionine aminopeptidase-2 based on a 1,2,4-triazole pharmacophore. J Med Chem 50(16):3777–3785. https://doi.org/10.1021/jm061182w

32. Morgen M et al (2016) Spiroepoxytriazoles are fumagillin-like irreversible inhibitors of MetAP2 with potent cellular activity. ACS Chem Biol 11(4):1001–1011. https://doi.org/10.1021/acschembio.5b00755

33. Mysinger MM et al (2012) Directory of useful decoys, enhanced (DUD-E): better ligands and decoys for better benchmarking. J Med Chem 55(14):6582–6594. https://doi.org/10.1021/jm300687e

34. Kurogi Y, Guner O (2001) Pharmacophore modeling and three-dimensional database searching for drug design using catalyst. Curr Med Chem 8(9):1035–1055. https://doi.org/10.2174/0929867043364036

35. Sterling T, Irwin JJ (2015) ZINC 15 – ligand discovery for everyone. J Chem Inf Model 55(11):2324–2337. https://doi.org/10.1021/acs.jcim.5b00559

36. Lipinski CA (2004) Lead- and drug-like compounds: the rule-of-five revolution. Drug Discov Today Technol 1(4):337–341. https://doi.org/10.1016/j.ddtec.2004.11.007

37. Bhal SK et al (2007) The rule of five revisited: applying log D in place of log P in drug-likeness filters. Mol Pharm 4(4):556–560. https://doi.org/10.1021/mp0700209

38. Morris GM et al (2009) AutoDock4 and AutoDockTools4: automated docking with selective receptor flexibility. J Comput Chem 30(16):2785–2791. https://doi.org/10.1002/jcc.21256

39. Yang H et al (2019) admetSAR : web-service for prediction and optimization of chemical ADMET properties. Bioinformatics 35(6):1067–1069. https://doi.org/10.1093/bioinformatics/bty707

40. Lee J et al (2015) CHARMM-GUI input generator for NAMD, GROMACS, AMBER, OpenMM, and CHARMM/OpenMM simulations using the CHARMM36 additive force field. J Chem Theory Comput 12(1):405–413. https://doi.org/10.1021/acs.jctc.5b00935

41. Kim S et al (2017) CHARMM-GUI ligand reader and modeler for CHARMM force field generation of small molecules. J Comput Chem 38(21):1879–1886. https://doi.org/10.1002/jcc.24829

42. Phillips JC et al (2005) Scalable molecular dynamics with NAMD. J Comput Chem 26(16):1781–1802. https://doi.org/10.1002/jcc.20289

43. Pettersen EF et al (2004) UCSF chimera—a visualization system for exploratory research and analysis. J Comput Chem 25(13):1605–1612. https://doi.org/10.1002/jcc.20084

44. Ahmed HEA, Zayed MF, Ihmaid S (2015) Molecular pharmacophore selectivity studies, virtual screening, and in silico ADMET analysis of GPCR antagonists. Med Chem Res 24(9):3537–3550. https://doi.org/10.1007/s00044-015-1389-6

45. Uba AI, Yelekçi K (2018) Pharmacophore-based virtual screening for identification of potential selective inhibitors of human histone deacetylase 6. Comput Biol Chem 77:318–330. https://doi.org/10.1016/j.compbiolchem.2018.10.016

46. Sakkiah S et al (2014) Dynamic and multi-pharmacophore modeling for designing polo-box domain inhibitors. PLoS ONE 9(7):e101405. https://doi.org/10.1371/journal.pone.0101405

47. van Breemen RB, Li Y (2005) Caco-2 cell permeability assays to measure drug absorption. Expert Opin Drug Metab Toxicol 1(2):175–185. https://doi.org/10.1517/17425255.1.2.175

48. Hewitt M et al (2009) In silico prediction of aqueous solubility: the solubility challenge. J Chem Inf Model 49(11):2572–2587. https://doi.org/10.1021/ci900286s

49. Schultes S et al (2010) Ligand efficiency as a guide in fragment hit selection and optimization. Drug Discov Today Technol 7(3):e157–e162. https://doi.org/10.1016/j.ddtec.2010.11.003

50. Uba AI et al (2019) Examining the stability of binding modes of the co-crystallized inhibitors of human HDAC8 by molecular dynamics simulation. J Biomol Struct Dyn. https://doi.org/10.1080/07391102.2019.1615989

51. Kleinjung J, Martínez L (2015) Automatic identification of mobile and rigid substructures in molecular dynamics simulations and fractional structural fluctuation analysis. Plos One. https://doi.org/10.1371/journal.pone.0119264

Authors and Affiliations

Safana Albayati[1] · Abdullahi Ibrahim Uba[1,2] · Kemal Yelekçi[1]

✉ Kemal Yelekçi
yelekci@khas.edu.tr

1. Department of Bioinformatics and Genetics, Faculty of Engineering and Natural Science, Kadir Has University, 34083 Cibali Campus Fatih, Istanbul, Turkey

2. Complex Systems Division, Beijing Computational Science Research Center, Beijing 100193, China